Optics Letters

Multidimensional synthetic frequency lattice in the dynamically modulated waveguides

Zhuoxiong Liu,[1] Lingzhi Zheng,[1] Chengzhi Qin,[1,3] Bing Wang,[1,*] and Peixiang Lu[1,2,4]

[1]School of Physics and Wuhan National Laboratory for Optoelectronics, Huazhong University of Science and Technology, Wuhan 430074, China
[2]Hubei Key laboratory of Optical Information and Pattern Recognition, Wuhan Institute of Technology, Wuhan 430025, China
[3]qinchengzhi@hust.edu.cn
[4]lupeixiang@hust.edu.cn
*wangbing@hust.edu.cn

Received 27 March 2023; revised 12 May 2023; accepted 13 May 2023; posted 15 May 2023; published 5 June 2023

Here we propose an effective method to construct a higher-dimensional synthetic frequency lattice with an optical waveguide under dynamic modulation. By applying the traveling-wave modulation of refractive index modulation with two different frequencies that are not mutually commensurable, a two-dimensional frequency lattice could be formed. The Bloch oscillations (BOs) in the frequency lattice is demonstrated by introducing a wave vector mismatch of the modulation. We show that the BOs are reversible only as the amounts of wave vector mismatch in orthogonal directions are mutually commensurable. Finally, by employing an array of waveguides with each under traveling-wave modulation, a 3D frequency lattice is formed and its topological effect of one-way frequency conversion is revealed. The study offers a versatile platform for exploring higher-dimensional physics in concise optical systems and may find great application in optical frequency manipulations.

https://doi.org/10.1364/OL.491680

The recently proposed concept of synthetic dimension provides a versatile platform to explore topological physics, which has been implemented in cold atoms [1,2], micro-ring resonators [3,4], and waveguide systems [5,6]. There are generally two approaches for creating the synthetic dimension. One approach involves coupling the internal degree of freedom of particles to form a synthetic lattice system. The other approach is to exploit the parameter dependency of the system. In the last decade, numerous methods have been proposed to create the synthetic dimension, such as guided modes with different angular momentum in a degenerate optical cavity [7], coupled super-modes with different propagation constants in a curved waveguide array [8], and optical pulses in a coupled fiber loops system [9]. Specifically, to create a synthetic frequency dimension, one could introduce the refractive index modulations into a photonic ring resonator or a dielectric waveguide [10], both of which couple the modes with different frequencies, thus forming a synthetic frequency lattice.

Generally, the physics of a photonic structure is tied to its geometric dimensionality. For a frequency lattice, by manipulating the waveform format that controls the modulators, the dimensionality of the lattice can be precisely controlled, resulting in unique physical properties. A one-dimensional (1D) frequency lattice is created by applying single-frequency refractive index modulation [11,12]. The construction of a higher-dimensional frequency lattice traditionally involves introducing long-range couplings [13], which are achieved by applying additional modulations with frequencies that are integral multiples of the original modulation. However, because of the presence of long-range coupling, the generated lattice is imposed by the twist boundary condition, which inevitably limits the independency of the lattice along orthogonal directions.

Here, we propose an effective method to construct higher-dimensional frequency lattices in modulated waveguides. We demonstrate that a two-dimensional (2D) frequency lattice can be created by applying traveling-wave refractive index modulation with two frequencies that are not mutually commensurable. A relevant work which creates a higher-dimensional Floquet lattice in a spin 1/2 particle system also employs this idea [14]. By introducing the wave vector mismatch, we generate a 2D effective force in the 2D frequency lattice and investigate the unique features of lattice dynamics under this force. Moreover, by precisely controlling the modulation phases and combining the 2D lattice with one spatial dimension, we create a 3D frequency lattice and demonstrate its topological effects for one-way frequency conversion.

We start with a dielectric waveguide under refractive index modulation $n = n_0 + \Delta n_1 \cos(\Omega_1 t - q_1 z + \phi_1) + \Delta n_2 \cos(\Omega_2 t - q_2 z + \phi_2)$, as shown in Fig. 1(a), where Ω_1 and Ω_2 are two noncommensurable modulations. The electric field in the waveguide can be expressed as $E(z, t) = \sum a_{m,n}(z, t) \exp[i(\omega_{m,n} t - \beta_{m,n} z)]$, where $a_{m,n}(z, t)$ is the mode amplitude with frequency $\omega_{m,n} = \omega_0 + m\Omega_1 + n\Omega_2$ and wave vector $\beta_{m,n} = \beta_0 + mq_1 + nq_2$. By applying the slow-varying amplitude approximation, we obtain the coupled-mode equation which is given by

$$i\frac{\partial a_{m,n}}{\partial z} = C_1 e^{-i\phi_1} a_{m+1,n} + C_1 e^{i\phi_1} a_{m-1,n} + C_2 e^{-i\phi_2} a_{m,n+1} + C_2 e^{i\phi_2} a_{m,n-1}, \quad (1)$$

where $C_{1,2} = \Delta n_{1,2}\omega_0/2c$ is the coupling strength. Equation (1) describes a particle on a 2D square lattice with nearest-neighbor coupling, where the two orthogonal directions are $\omega 1$ and ω_2

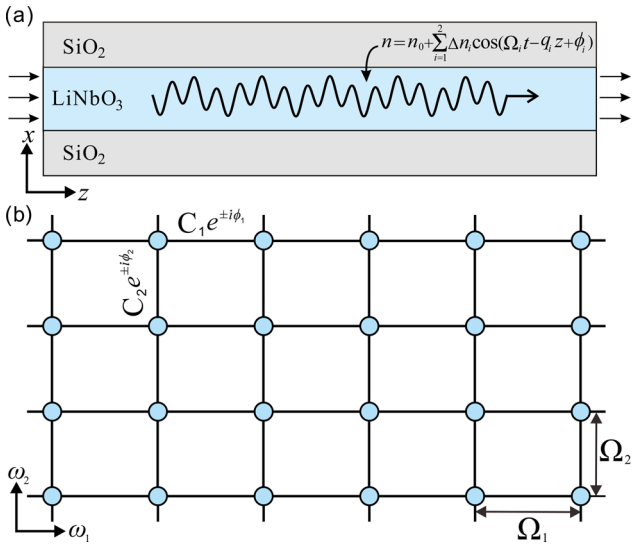

Fig. 1. (a) Schematic of the waveguide under dual-frequency refractive index modulation with Ω_1 and Ω_2 being modulation frequencies. The curve represents the traveling-wave modulation. The materials of the core and cladding are SiO_2 and $LiNbO_3$. (b) Equivalent 2D frequency lattice model with lattice constants Ω_1 and Ω_2. Two orthogonal directions here are ω_1 and ω_2. The coupling coefficients of two orthogonal directions are $C_1\exp(\pm i\phi_1)$ and $C_2\exp(\pm i\phi_2)$.

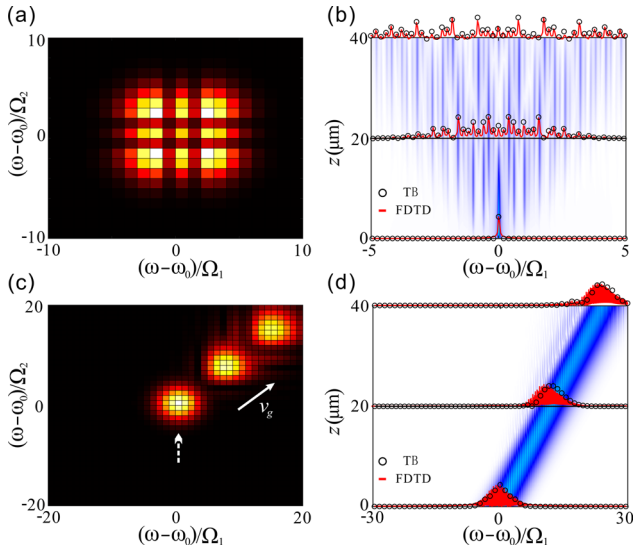

Fig. 2. (a) Normalized intensity distributions on the 2D frequency lattice at $z = 40\,\mu m$ for the single-frequency excitation. (b) Complete spectrum evolutions for the single-frequency excitation. The black circles and red curves symbolize the results of tight-binding and FDTD methods. (c) Normalized intensity distributions on the 2D frequency lattice at $z = 0$, 20, 40 μm for the Gaussian profile excitation. Here, v_g represents the group velocity of the wave packet. (d) Corresponding complete spectrum evolutions of the Gaussian profile excitation.

due to the independence of the two modulation frequencies. The creation process of this lattice can be visualized as follows: imagine injecting a mode with frequency ω_0 into the modulated waveguide. Then the modulation with frequency Ω_1 would induce the appearance of modes with frequency $\omega = \omega_0 + m\Omega_1$. The modulation with frequency Ω_2 further excites modes with frequency $\omega = \omega_0 + m\Omega_1 + n\Omega_2$, forming a 2D lattice as shown in Fig. 1(b). The integers m and n represent the site index of two orthogonal directions and the couplings along the horizontal and vertical directions are caused by modulations with frequencies Ω_1 and Ω_2, respectively. Therefore, the lattice sites of the 2D frequency lattice are waveguide modes with frequency $\omega_{m,n} = \omega_0 + m\Omega_1 + n\Omega_2$. As long as the two modulation frequencies are not mutually commensurable, the frequencies of excited modes do not repeat, resulting in a truly infinite 2D lattice.

To validate the accuracy of our 2D lattice model, we perform the simulations using both the tight-binding and finite-difference time-domain (FDTD) methods to analyze the spectral evolution of single-site and Gaussian profile excitations. The results of the single-site excitation are displayed in Figs. 2(a) and 2(b), which show the normalized intensity distribution on the 2D frequency lattice at $z = 40\,\mu m$ and the corresponding complete spectrum evolutions, respectively. The single-site excitation can be considered as a uniform excitation across the entire band in k-space, resulting in a phenomenon termed as discrete diffraction. In particular, Fig. 2(b) displays the spectrum distributions obtained from the tight-binding and FDTD methods at $z = 0\,\mu m$, 20 μm, and 40 μm, denoted by the red curves and black circles. The results from both methods exhibit good agreement, indicating the correctness of Eq. (1). Figures 2(c) and 2(d) depict the results for the Gaussian profile excitation. This type of excitation only excites a portion of the band, causing it to travel in a specific direction determined by the corresponding group velocity.

By introducing the wave vector mismatch in the modulations, an effective electric force can be created in the frequency lattice, which gives rise to the phenomenon known as Bloch oscillations (BOs). This idea has been explored in 1D frequency lattice [11,15–17]. Here we generalize this to a 2D lattice and investigate its unique features. To incorporate the mismatch, the format of refractive index modulation needs to be modified as $n = n_0 + \Delta n_1\cos(\Omega_1 t - q_1 z - \Delta q_1 z + \phi_1) + \Delta n_2\cos(\Omega_2 t - q_2 z - \Delta q_2 z + \phi_2)$, where Δq_1 and Δq_2 indicate the wave vector mismatch. Now the band structure of the system is expressed as

$$k_z' = 2C_1\cos(k_{\omega_1}\Omega_1 - \phi_1 + \Delta q_1 z) + 2C_2\cos(k_{\omega_2}\Omega_2 - \phi_2 + \Delta q_2 z). \quad (2)$$

Equation (2) actually describes a particle on a two-dimensional lattice subject to an effective force $F = -\Delta q_1/\Omega_1\, \boldsymbol{i} - \Delta q_2/\Omega_2\, \boldsymbol{j}$, where $\boldsymbol{i}$ and $\boldsymbol{j}$ denote unit vector along the ω_1 and ω_2 axes, respectively. Therefore, by adjusting Δq_1 and Δq_2, the strength and direction of the effective force can be manipulated, ultimately affecting the lattice dynamics. To characterize this more vividly, we consider the spectrum evolutions of a Gaussian profile wave packet in the presence of an effective force. According to Eq. (2), the frequency shifts $\Delta\omega$ at the specific evolution distance z_S are expressed as

$$\begin{aligned}\Delta\omega = {} & 2[\cos(k_{\omega_1}\Omega_1 - \phi_1 + \Delta q_1 z_s) - \cos(k_{\omega_1}\Omega_1 - \phi_1)]C_1\Omega_1/\Delta q_1 \\ & +2[\cos(k_{\omega_2}\Omega_2 - \phi_2 + \Delta q_2 z_s) - \cos(k_{\omega_2}\Omega_2 - \phi_2)]C_2\Omega_2/\Delta q_2. \end{aligned} \quad (3)$$

For a 1D frequency lattice, the last term in Eq. (3) will vanish so that there always exists an oscillation period $z_T = 2\pi/\Delta q_1$ where the frequency shift $\Delta\omega$ is zero. For the 2D case, however, the condition for $\Delta\omega = 0$ is expressed as

$$\begin{cases}\cos(k_{\omega_1}\Omega_1 - \phi_1 + \Delta q_1 z_s) - \cos(k_{\omega_1}\Omega_1 - \phi_1) = 0 \\ \cos(k_{\omega_2}\Omega_2 - \phi_2 + \Delta q_2 z_s) - \cos(k_{\omega_2}\Omega_2 - \phi_2) = 0. \end{cases} \quad (4)$$

Equation (4) holds true only if $\Delta q_1/\Delta q_2 = M/N$, where M and N are arbitrary non-zero integers. This means that the spectrum

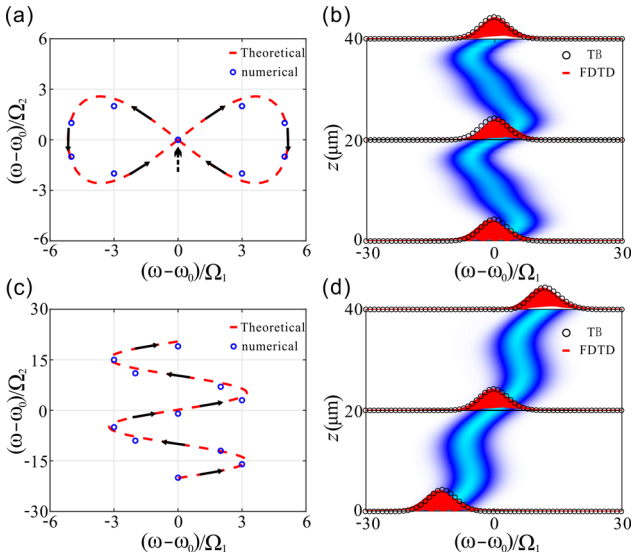

Fig. 3. (a) Central frequency evolutions of the Gaussian profile wave packets on the 2D frequency lattice with $\Delta q_2 = 2\Delta q_1$. The blue circles and red dashed curve represent the numerical and theoretical results. (b) Corresponding complete spectrum evolution process. (c),(d) Central frequency and total spectrum evolutions with $\Delta q_2 = 0$.

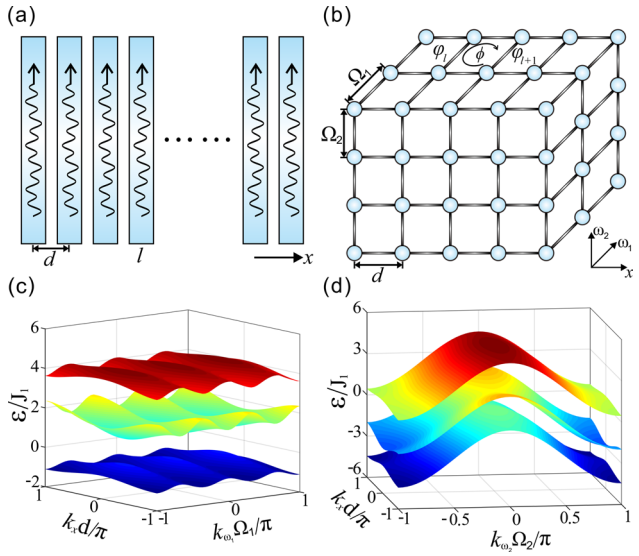

Fig. 4. (a) Schematic of the 1D waveguide array. The distance between adjacent waveguide is d. The lth waveguide undergoes a modulation with phase φ_l. (b) Equivalent synthetic lattice model with three mutually orthogonal directions x, ω_1, ω_2. The lattice constants are d, Ω_1, and Ω_2, respectively. A loop encircling a single plaquette in the x–ω_1 plane is associated with a phase shift ϕ, which indicates the presence of an effective magnetic field. (c),(d) Projected band structures as a function of (k_x, $k_{\omega 1}$) and (k_x, $k_{\omega 2}$), respectively.

pattern is reversible only if the modulation wave vector mismatches are mutually commensurable. Figure 3(a) displays the central frequency evolutions of a Gaussian profile wave packet, where we set $\Delta q_2 = 2\Delta q_1$. The blue circles and red dashed curves in Fig. 3(a) represent the numerical and theoretical results, respectively. The central frequency oscillates and returns to its original value after an oscillation period, indicating the recoverability of the spectrum. Figure 3(b) shows the complete frequency spectrum evolution process, and the recoverability of spectrum pattern is also displayed clearly. In Figs. 3(c) and 3(d), we set Δq_2 to zero, so the condition for $\Delta\omega = 0$ is not satisfied. The vanishing of Δq_2 means that the effective force along the ω_2 axis is zero so that the central frequency of the wave packet travels along the positive direction of ω_2 and oscillates along the ω_1 axis simultaneously. As a result, the central frequency cannot recover to its original value.

To enhance the robustness of the spectral manipulation, we are going to investigate the topological effects of a 1D dynamically modulated waveguide array. As shown in Fig. 4(a), the array comprises uniform waveguides separated by a fixed distance of d. Each waveguide undergoes a dual-frequency refractive index modulation, $n = n_0 + \Delta n_1 \cos(\Omega_1 t - q_1 z + \varphi_l) + \Delta n_2 \cos(\Omega_2 t - q_2 z)$, where φ_l is the associated modulation phase at the lth waveguide. As explained above, this type of modulation induces a 2D frequency lattice in each waveguide. Combined with the spatial dimension, as shown in Fig. 4(b), the equivalent lattice model of this structure is a 3D lattice with three mutually orthogonal directions: x, ω_1, ω_2. The lattice constants correspond to the waveguide spacing and two modulation frequencies, respectively. The Hamiltonian of the system is given by

$$H = \sum_{m,n,l} C_1 e^{-i\varphi_l} a^+_{m,n,l} a_{m+1,n,l} + C_2 a^+_{m,n,l} a_{m,n+1,l} + C_s a^+_{m,n,l} a_{m,n,l+1} + h.c., \tag{5}$$

where C_S, C_1, and C_2 are coupling strengths along the x, ω_1, and ω_2 axes, respectively. The modulation phase φ_l would induce a nonreciprocal phase term in the coupling along ω_1 direction, as described by the first term in Eq. (5). Therefore, as depicted in Fig. 4(b), a loop encircling a single plaquette in the x–ω_1 plane is associated with a phase shift ϕ, which is analogous with the geometric phase acquired by a charged particle in a constant magnetic field piercing the lattice [18,19]. Therefore, Eq. (5) actually describes a 3D system labeled by (m, n, l), which consists of layers of the Harper–Hofstadter model stacked along the ω_2 axis. By applying the Landau gauge $\varphi_l = l \cdot 2\pi/3$ for a uniform field, we can rewrite Eq. (5) into k-space as

$$\begin{aligned} H(k) = \sum_{i=1}^{3} \{ & C_s (a^+_{k,i} a_{k,i+1} e^{ik_x d} + a^+_{k,i+1} a_{k,i} e^{-ik_x d}) \\ & + [2C_1 \cos(k_{\omega_1}\Omega_1 - \varphi_i) + 2C_2 \cos k_{\omega_2}\Omega_2] a^+_{k,i} a_{k,i} \}, \end{aligned} \tag{6}$$

where $\varphi_i = 2\pi/3,\ 4\pi/3,\ 2\pi$, respectively. We calculate the band structure defined as eigenvalues of Eq. (6) and the band structures projected to $k_x - k_{\omega 1}$ and $k_x - k_{\omega 2}$ planes are displayed in Figs. 4(c) and 4(d). The topology of the system is featured by a triad of topological index $C = (C_x, C_{\omega 1}, C_{\omega 2})$, where C_i ($i = x$, ω_1, ω_2) is the first Chern number of the 2D momentum plane normal to the i axis [20]. For all the bands, the values of C_x and $C_{\omega 1}$ are zero. However, the values of $C_{\omega 2}$ of three bands from top to bottom are -1, 2, -1, which indicates the non-trivial topology of our synthetic lattice system.

The non-trivial topology of a finite lattice is reflected in the emergence of topological surface states. As an illustration, we consider a system with 25 waveguides. In each waveguide, the modulation phase φ_l takes the form of $\varphi_l = |l - l_0| \cdot 2\pi/3$, where $l_0 = 13$ represents the site number of the central waveguide. This arrangement creates the effective magnetic field with opposite

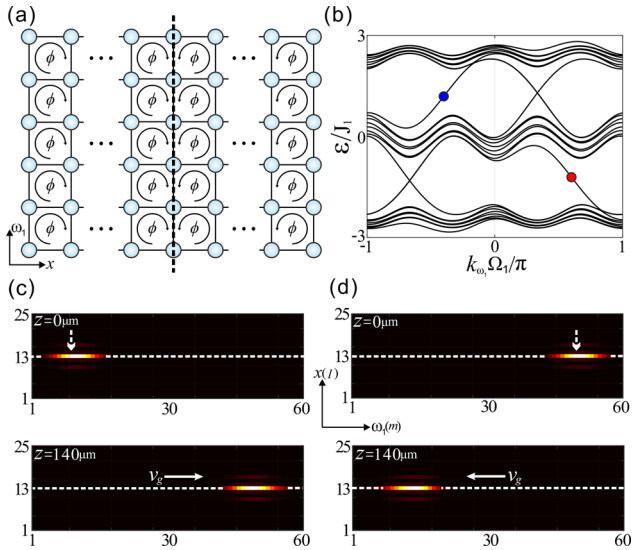

Fig. 5. (a) Schematic of the cross section of the 3D synthetic lattice. The dashed line represents the interface separating the 3D lattice structure. The directions of the effective magnetic fields on two sides are opposite. (b) Sliced projected band structures as a function of $k_{\omega 1}$ at $k_{\omega 2} = 0.5\pi/\Omega_2$. The blue and red spheres represent the gapless surface states shown in Figs. 5(c) and 5(d), respectively. (c),(d) Surface states evolutions in the x–ω_1 plane. The directions of the group velocities of two surface states along ω_1 are opposite, which indicates the opposite frequency shifts.

directions on two sides of the central waveguide, resulting in an interface separating the 3D lattice structure as indicated by the dashed line in Fig. 5(a). In particular, the Bloch momenta $k_{\omega 1}$ and $k_{\omega 2}$ are well defined due to the translational symmetry along ω_1 and ω_2 axes. The sliced projected band structure defined as a function of $k_{\omega 1}$ at $k_{\omega 2} = 0.5\pi/\Omega_2$ is shown in Fig. 5(b), where the gapless surface states in the bandgap are clearly manifested. Figures 5(c) and 5(d) demonstrate the unidirectional transmission characteristics of surface states. The excitation injected into the synthetic lattice is a 3D wave packet which takes the Gaussian profile distribution in the ω_1–ω_2 plane and decays rapidly along the x axis. The phase differences between adjacent sites are also adjusted carefully so that the Bloch momenta carried by the packet can be manipulated. In Fig. 5(c), the excited surface state is represented by the blue sphere shown in Fig. 5(b). The state travels along the positive direction of ω_1 unidirectionally while keeping localized at the interface of the lattice, which clearly manifests the transmission features of surface states. In the case of Fig. 5(d), the excited surface state is symbolized by a red sphere shown in Fig. 5(b). The group velocity direction is reversed now so that it would travel along the negative direction of ω_1.

In summary, we have shown that a traveling-wave refractive index modulation with two non-commensurable frequencies in a waveguide can induce a 2D frequency lattice. The method could be extended to create an arbitrary higher-dimensional frequency lattice. We introduce the modulation wave vector mismatches to display the BOs in a 2D frequency lattice and verify that the BOs become reversible when the mismatches are mutually commensurable in two orthometric directions. By combining the 2D frequency lattice with one spatial dimension, we create a 3D frequency lattice and display the unidirectional transmission features of topological surface states. In experiment, the cross talk of modulation signals between adjacent waveguides may affect the effectiveness of the lattice model. This impact could be reduced by employing the technique called digital precompensation which reduces the cross talk of modulation signal while not affecting the coupling of optical signals significantly. The study provides a versatile platform for exploring higher-dimensional physical phenomena in synthetic dimensions, and may have an impact on the exploration of topological photonics and optical wave manipulation in frequency domains.

Funding. National Natural Science Foundation of China (11974124, 12021004, 12204185).

Disclosures. The authors declare no conflicts of interest.

Data availability. Date underlying the results presented in this paper are not publicly available at this time but may be obtained from the authors upon reasonable request.

REFERENCES

1. Y. E. Kraus and O. Zilberberg, Phys. Rev. Lett. **109**, 116404 (2012).
2. O. Boada, A. Celi, J. I. Latorre, and M. Lewenstein, Phys. Rev. Lett. **108**, 133001 (2012).
3. K. Wang, A. Dutt, C. C. Wojcik, and S. Fan, Nature **598**, 59 (2021).
4. A. Dutt, L. Yuan, K. Y. Yang, K. Wang, S. Buddhiraju, J. Vuckovic, and S. Fan, Nat. Commun. **13**, 3377 (2022).
5. C. Qin, F. Zhou, Y. Peng, D. Sounas, X. Zhu, B. Wang, J. Dong, X. Zhang, A. Alu, and P. Lu, Phys. Rev. Lett. **120**, 133901 (2018).
6. B. A. Bell, K. Wang, A. S. Solntsev, D. N. Neshev, A. A. Sukhorukov, and B. J. Eggleton, Optica **4**, 1433 (2017).
7. X. W. Luo, X. Zhou, C. F. Li, J. S. Xu, G. C. Guo, and Z. W. Zhou, Nat. Commun. **6**, 7704 (2015).
8. E. Lustig, S. Weimann, Y. Plotnik, Y. Lumer, M. A. Bandres, A. Szameit, and M. Segev, Nature **567**, 356 (2019).
9. A. Regensburger, C. Bersch, M. A. Miri, G. Onishchukov, D. N. Christodoulides, and U. Peschel, Nature **488**, 167 (2012).
10. L. Yuan, Q. Lin, M. Xiao, and S. Fan, Optica **5**, 1396 (2018).
11. C. Qin, L. Yuan, B. Wang, S. Fan, and P. Lu, Phys. Rev. A **97**, 063838 (2018).
12. Y. Hu, M. Yu, N. Sinclair, D. Zhu, R. Cheng, C. Wang, and M. Loncar, Nat. Commun. **13**, 6293 (2022).
13. L. Yuan, M. Xiao, Q. Lin, and S. Fan, Phys. Rev. B **97**, 104105 (2018).
14. I. Martin, G. Refael, and B. Halperin, Phys. Rev. X **7**, 041008 (2017).
15. L. Yuan and S. Fan, Optica **3**, 1014 (2016).
16. H. Chen, N. Yang, C. Qin, W. Li, B. Wang, T. Han, C. Zhang, W. Liu, K. Wang, H. Long, X. Zhang, and P. Lu, Light: Sci. Appl. **10**, 48 (2021).
17. W. Li, C. Qin, T. Han, H. Chen, B. Wang, and P. Lu, Opt. Lett. **44**, 5430 (2019).
18. K. Fang, Z. Yu, and S. Fan, Nat. Photonics **6**, 782 (2012).
19. L. Yuan, Y. Shi, and S. Fan, Opt. Lett. **41**, 741 (2016).
20. M. Kim, Z. Jacob, and J. Rho, Light: Sci. Appl. **9**, 130 (2020).